Mesojunction-based design paradigm of structural DNA nanotechnology

Tianqi Wang^{1,#}, Tanxi Bai^{1,#}, Zhenyu Tan¹, Yoel P. Ohayon^{2,*}, Ruojie Sha², Simon Vecchioni², Nadrian C. Seeman^{2†}, Bryan Wei^{1,*}

Abstract

Mesojunctions were introduced as a basic type of crossover configuration in the early development of structural DNA nanotechnology. However, the investigations of self-assembly from multiple mesojunction complexes have been overlooked in comparison to their counterparts based on regular junctions. In this work, we designed standardized component strands for the construction of complex mesojunction lattices. Three typical mesojunction configurations with three and four arms were showcased in the self-assembly of 1-, 2- and 3-dimensional lattices constructed from both a scaffold-free tiling approach and a scaffolded origami approach.

Introduction

Various junction and crossover motifs have been identified in the field, particularly during the early development of structural DNA nanotechnology when theoretical studies predominated¹. By the mid 1990's, architectures based on 3-arm and 4-arm regular junctions became dominant in the development of DNA nanotechnology²⁻¹³. Notably, in the design of compact-helix-based, two-dimensional (2D) and three-dimensional (3D) origami that has become prevalent, all crossover schemes are derived from 4-arm regular junctions¹⁴⁻¹⁶. More recently, several architecture frameworks emerged for the design and construction of wireframe DNA nanostructures¹⁷⁻²⁰ and, without exception, they are all based on regular junctions that employ different numbers of double helical arms.

According to the nomenclature used in earlier reports²¹, a branched DNA junction contains duplexes radiating from a central junction point (Figure. 1a, left and middle); an antijunction, on the contrary, is comprised of duplexes pointing in a circumferential direction (Figure, 1a, right); a mesojunction mixes both radial duplexes and circumferential duplexes flanking a central point (Figure. 1b). We use X_Y/Z_{X_Y} as a nomenclature to describe a certain junction configuration (e.g., regular junction, antijunction and mesojunction), where X represents the total number of strands involved, Y the number of radial duplex arms, and Z the index number of configuration variants. The 3-arm and the 4-arm DNA junctions are termed as 3₃ and 4₄ respectively because either all three or four duplexes are radial²¹. Likewise, the 4arm antijunction is termed as 40 because no radial arm is present (i.e., all four arms are circumferential)²¹. An antijunction with three arms cannot be constructed due to the restriction imposed by strand polarity (Figure, S1). Only the 3₁ mesojunction configuration can be designed from the 3-arm junction, consisting of one radial arm and two circumferential arms (Figure. 1b, left)²¹. Two different configurations are available for the 4-arm design with two radial arms and two circumferential arms (Figure. 1b, middle and right) — the ¹4₂ mesojunction, comprising alternating radial arms and circumferential arms, and the ²4₂ mesojunction, comprising pairwise radial arms and circumferential arms²¹.

The formation of basic multi-stranded mesojunction complexes has previously been investigated^{21, 22}, but the self-assembly of multiple mesojunction complexes into periodic lattices remained unrealized since their introduction²³. Here, we carried on this unfinished task by designing the standardized component strands for our self-assembly investigation of mesojunction lattices. We first designed and constructed one-dimensional (1D) periodic lattices based on 3-arm and 4-arm mesojunctions using the three typical mesojunction configurations, 3₁, ¹4₂, and ²4₂. We then applied mesojunction architecture in the self-assembly of discrete lattices. We adopted the ¹4₂ mesojunction to construct rectangles of defined dimensions using both a scaffold-free tiling approach as well as a scaffolded DNA origami approach. Besides single duplex arms, we designed two bundled duplexes as a composite arm for 2D and 3D mesojunction lattices. Our successful self-assembly that resulted in various mesojunction

¹School of Life Sciences, Tsinghua University-Peking University Center for Life Sciences, Center for Synthetic and Systems Biology, Tsinghua University, Beijing 100084, China.

²Department of Chemistry, New York University, New York, New York 10003, USA

^{*}These authors contributed equally. †Deceased.

^{*}Corresponding Author. Email: bw@tsinghua.edu.cn (B.W.); yoel.ohayon@nyu.edu (Y.P.O.).

lattices presents the mesojunction architecture as a general design scheme to produce complex DNA nanostructures.

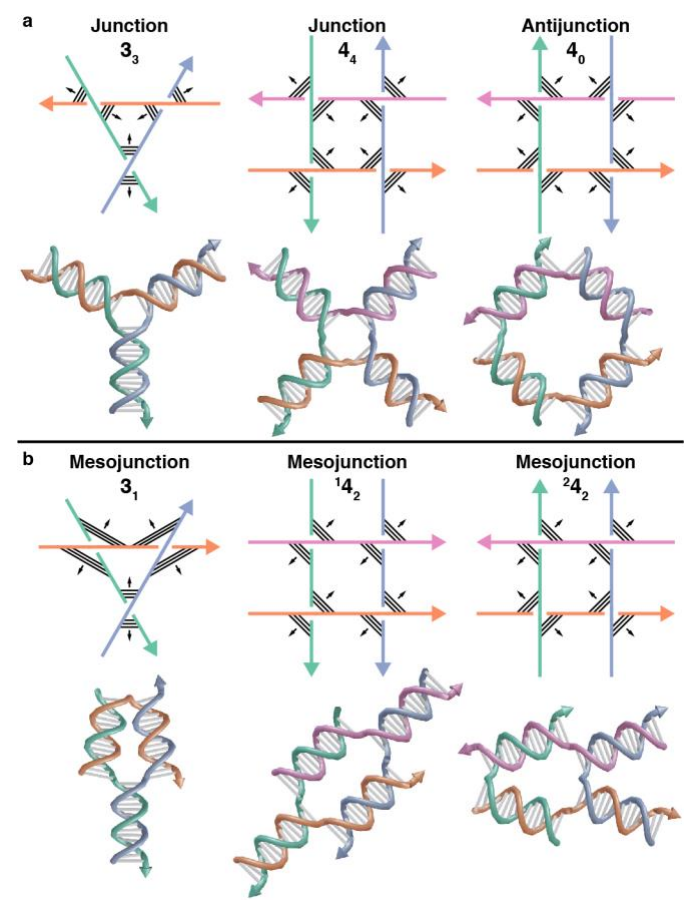


Figure. 1. Schematics of canonical DNA junctions, antijunctions and mesojunctions. Solid lines depict the antiparallel DNA backbones and arrowheads denote the 3' ends of the strands. Thin parallel lines indicate base pairs between DNA strands. (a) Schematic drawings of 3₃ (left) and 4₄ (middle) junctions and 4₀ antijunction (right). The axis of each one-half-turn duplex is represented by the central dyad arrows perpendicular to the base pairs, which is either pointing radially towards the center (junction) or circumferential about a center (antijunction). (b) Schematic drawings of 3₁ (left), ¹4₂ (middle) and ²4₂ (right) mesojunctions, respectively. Top panels: schematics of complexes with one half-turn between crossovers. Bottom panels: schematics of complexes with three half-turns between crossovers, which readily illustrate the strand weaving across DNA duplexes.

Results

1D periodic mesojunction lattices

We began our self-assembly investigation with a set of 1D periodic lattices based on the three typical 3_1 , 14_2 and 24_2 mesojunctions. Standardized component strands with common segmentation were designed for the lattice construction.

We first sought to design and construct periodic structures based on the $^{1}4_{2}$ mesojunction. A 4-arm complex with an arm length of three half-turns (i.e., 16 base pairs) was initially tested as a model system (Figure. 2a). Specifically, a typical component strand contains 32 nucleotides (nt) with three consecutive binding domains (A, B and C). The 16-nt center domain B propagates through an entire arm, and the 8-nt 5'-domain A and the 8-nt 3'-domain C cross to the neighboring arms. As shown in Figure 2a, we designed a 6-helix ribbon composed of 12 addressable component strands (8 core strands and 4 boundary strands, see Figure. S2 for detailed designs). With a fixed width of six helices, the 1D periodic lattice was designed to extend along the helical direction. Collectively, diagonally oriented component strands pair with partner strands of the opposite direction, forming the basis for a rectangular wave geometry (Figure. 2a, top left panel). The successful formation of the periodic ribbons was confirmed by atomic force microscopy (AFM), and the width of the ribbons was measured at 19 ± 3

nm under AFM, which agreed with the expected width ranging from 12 nm to 24 nm (a compact stacking state and a loose stacking state respectively; Supporting Note S1). The overall lattice size and deposition density under AFM remained limited even after many rounds of assembly optimization (Figure. 2a, right panel; Figure. S3). Presumably, the weak interaction of the 8-bp binding domains could lead to challenges in the assembly, so we then turned to an arm length design of four half-turns (21 bp) with longer binding domains (Figure. 2b). The design of standardized 42-nt component strands, with a 21-nt center domain B, a 10-nt 5'-domain A and an 11-nt 3'-domain C, points to a horizontal zigzag weaving topology (Figure. S4) instead of a diagonal zigzag for an arm length of three half-turns (Figure. S3), and similar pattern correspondence can also be found in the regular junction-based lattices¹. We characterized the design of four half-turns under AFM, and such a design yielded ribbons of 19 ± 3 nm, in good agreement with the designed width range (12 nm - 24 nm). A higher self-assembly yield was obtained for the design of four half-turns when compared to that of three half-turns (Figure. S5). Therefore, designs of both four and six half-turns were adopted in the lattices presented below.

Our attempt of constructing a wider ribbon (12 helices) led to an incomplete assembly in the direction perpendicular to the DNA axis, underscoring the difficulty of component strands being incorporated along the lateral direction (Figure. S6). We also aimed at assembling 2D lattices that extended indefinitely in both the helical and lateral directions. Due to the same assembly constraint of the wider ribbons and a possible tubulation along the lateral direction, 2D periodic lattices were not observed under either AFM or transmission electron microscopy (TEM) (Figure. S7).

We then sought to investigate the self-assembly of a 6-helix lattice of 24_2 mesojunction with four half-turns (Figure. 2c). Likewise, the 21-nt center domain B propagates throughout an entire circumferential arm, and the 10-nt 5'-domain A and the 11-nt 3'-domain C cross to the neighboring arms. The repetitive unit contained 12 addressable component strands (8 core strands and 4 boundary strands, see Figure. S8 for detailed designs). A herringbone geometry was observed in the 24_2 design. (Figure. 2c, top left panel). According to the morphology characterization under AFM, the resulting lattice adopted the expected width $(22 \pm 3 \text{ nm})$ and zigzag boundaries.

In addition to the 4-arm mesojunctions, we further investigated the self-assembly of periodic lattices from the 3₁ mesojunction (Figure. 2d). A special hybrid design of mesojunctions and regular junctions was adopted to cope with the routing challenge. We applied a similar principle to design 36 standardized component strands for a 12-helix lattice (see Figure. S9 for detailed designs). As shown in Figure 2D, we observed the formation of spiral lattices, presumably induced by the unintentional twist of the repeating units. Other lattice designs of 3₁ mesojunction were tested but no apparent lattices were observable under AFM (Figure. S10).

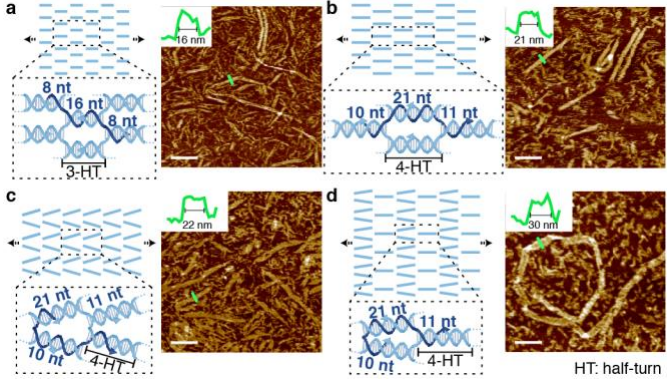


Figure. 2. 1D periodic lattices of 3-arm and 4-arm mesojunctions. (a) Periodic ribbon from the ¹4₂ mesojunction with an arm length of three half-turns. (b-d) Periodic lattices with four-half-turn arms using ¹4₂, ²4₂, and 3₁ mesojunctions, respectively. Top left panels: schematic diagrams of duplex arrangement of the periodic lattices. The dyad axes indicate the growing direction. Bottom left panels: schematic diagrams of a representative mesojunction in the periodic lattices. A typical component strand is highlighted in dark blue. The domain and arm lengths are specified respectively. Right panels: representative AFM images (insets show the width measurement of a selected lattice). Scale bars: 100 nm.

Discrete mesojunction lattices

Encouraged by the successful results of periodic mesojunction lattices, we continued our exploration toward discrete lattices with individually addressable components (Figures. 3 and 4). We focused on

the 14_2 mesojunction with an even number of half-turns from a scaffold-free tiling design as well as a scaffolded origami design. We developed lattices based on single duplex arms (Figure. 3), as well as pairwise-bundled duplexes as composite arms (Figure. 4) for 2D and 3D mesojunction constructs. In our construction of discrete lattices by a scaffold-free tiling approach (Figure. 3a), the standardized domain design with a 42-nt component strand like the periodic lattice was adopted. For illustrative purposes, we defined each mesojunction arm as a fragmented helix, and used the number of helices of a structural block to represent the lattice width and the total number of half-turns along the helical direction to represent the lattice length. Specifically, 173 core strands and 39 boundary strands were designed for a 12-helix \times 64-half-turn (12H \times 64HT) rectangular lattice (Figure. S11). The successful formation of the lattice was confirmed by native agarose gel electrophoresis and the assembly yield was estimated at 32% (Figure. S12; Table S1; Supporting Note S2), and the AFM images of the resulting structures revealed the expected rectangular shape (Figure. 3a, bottom panel), which was measured at 44 ± 3 nm \times 126 ± 10 nm.

We then created discrete mesojunction lattices from a scaffolded DNA origami construct (Figure. 3b). The routing of a standardized 42-nt staple is like the one in the tiling approach. Of the four crossovers of a given mesojunction, two of them stem from the scaffold and the other two come from the staple strands (Figure. 3b, middle panel). The routing scheme can be viewed as the scaffolded duplexes stitched by the scaffold-free ones. We designed a $23H \times 84HT$ lattice with 314 standardized staple strands (Figure. S13). The gel results pointed to the successful formation of the lattice with a high yield of 82% (Figure. S14). As shown in the AFM images (Figure. 3b, bottom panel), the $23H \times 84HT$ lattice took a desired rectangular morphology with the expected dimensions ($79 \pm 5 \text{ nm} \times 147 \pm 8 \text{ nm}$).

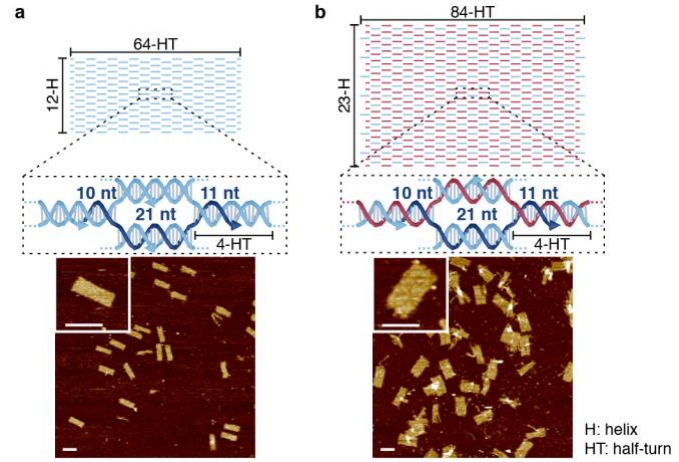


Figure. 3. 2D discrete lattices of $^{1}4_{2}$ mesojunction with four half-turns. (a) $12H \times 64HT$ rectangular tile lattice. (b) $23H \times 84HT$ rectangular origami lattice. Top panels: schematic diagrams of duplex segments in the lattices. Scaffold-free duplexes are colored in light blue and scaffolded duplexes are colored in magenta. Middle panels: schematic diagrams of a representative $^{1}4_{2}$ mesojunction with four half-turns in the lattices. The component strands and staples are colored in light blue, and the scaffold strand is colored in magenta. One typical component strand or staple is highlighted in dark blue. The domain and arm lengths are specified respectively. Bottom panels: representative AFM images (insets show magnified views). Scale bars: 100 nm.

The individual arms of the mesojunction lattices up to this point were designed as single duplexes. As was described in previous structures with regular junctions and antijunctions^{8, 24}, a given arm can be designed as a bundled complex with more than one duplex for a composite mesojunction lattice. With that in mind, we designed several origami lattices with composite ¹4₂ mesojunctions whose arms are bundles of dual duplexes (Figure. 4). A dual duplex bundle can be viewed as two scaffold segments paired with two U-shaped staples (two domains of 16-nt) of opposite orientations, leading to an arm length of six half-turns. Here we used the number of bundled helices in the structural block to represent the lattice width and the total number of half-turns along the helical direction to represent the lattice length. Specifically, we constructed a 20H × 60HT rectangular lattice with 200 standardized staples (Figure. 4a; Figure. S15). With the scaffold zigzagging in a specific pattern, all the crossovers between bundled duplex arms are derived from the scaffold (Figure. 4a, middle panel). Successful self-assembly was verified by agarose gel (the assembly yield of 8%; Figure. S16). The obtained AFM images

confirmed the formation of the rectangular lattice (Figure. 4a, bottom panel), which was measured at 72 ± 5 nm \times 123 ± 7 nm.

We further extended this composite arm design scheme to 3D lattices. Using the number of bundled helices as width, the number of total half-turns as length, and the number of lattice layers as height, we constructed two lattices of different aspect ratio, a 6H × 48HT × 4H cuboid and a 10H × 32HT × 4H cuboid respectively (Figure. 4, b and c). Instead of adopting two-domain staples in the single-layer design, four-domain staples were designed for both intra-layer and inter-layer base paring. In the 6H × 48HT × 4H cuboid, a 66-nt component staple comprises four consecutive binding domains of 18-nt, 18-nt, 13-nt and 13-nt, with TpT spacers between the two 18-nt domains and the two 13-nt domains (Figure. 4b, middle panel; Figure. S17). Such a design produced a discernible product band on the gel and gave a 29% assembly yield (Figure, S18). Monodisperse particles with a desired shape were also characterized by TEM (Figure. 4b, bottom panel) with expected dimensions ($20 \pm 2 \text{ nm} \times 74 \pm 6 \text{ nm} \times 74$ 9 ± 1 nm). For the $10H \times 32HT \times 4H$ cuboid (Figure. 4c; Figure. S19), we adopted an arm length of four half-turns (21 bp) and adjusted the domain segmentation of component strands accordingly (8-nt, 8-nt, 13-nt and 13-nt domains). Agarose gel results confirmed the successful formation of the structure with an assembly yield of 21% (Figure. S20) and the TEM images showed that the designed constructs adopted the expected morphology (29 \pm 4 nm \times 50 \pm 4 nm \times 8 \pm 1 nm; Table S2) with different side views (Figure. 4c, bottom panel).

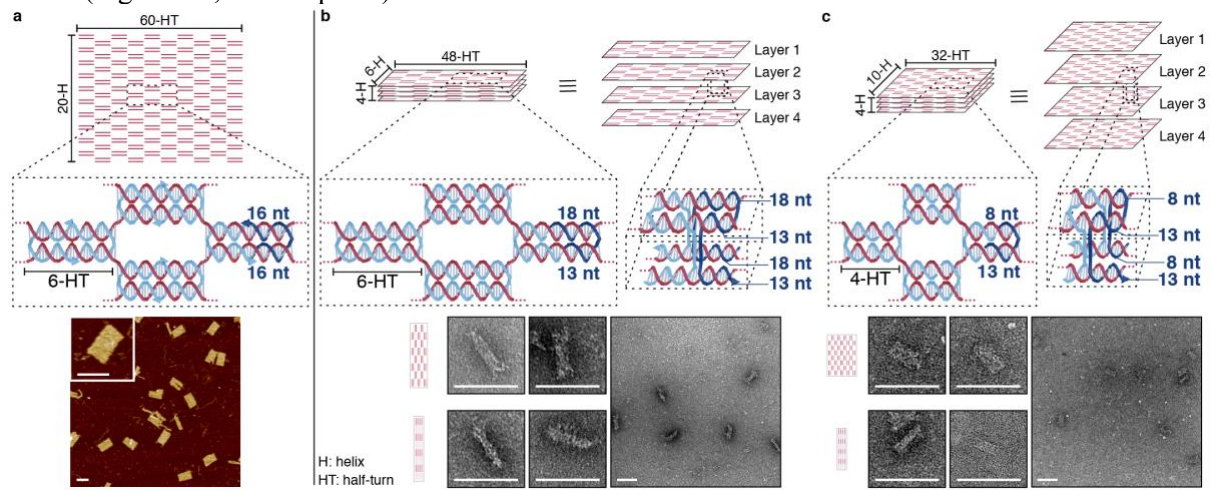


Figure. 4. 2D and 3D lattices of composite $^{1}4_{2}$ mesojunctions. (a) $20H \times 60HT$ rectangle of composite $^{1}4_{2}$ mesojunctions with six half-turns. (b) $6H \times 48HT \times 4H$ cuboid of composite $^{1}4_{2}$ mesojunctions with six half-turns. (c) $10H \times 32HT \times 4H$ cuboid of composite $^{1}4_{2}$ mesojunctions with four half-turns. Top panels: schematic diagrams of bundled duplex segments in the lattices. Middle panels: schematic diagrams of a representative composite $^{1}4_{2}$ mesojunction. The staples strands are colored in light blue and the scaffold strand is colored in magenta. One typical staple is highlighted in dark blue. The domain and arm lengths are specified respectively. Bottom panels: representative AFM images (insets show magnified views) and TEM images (left: zoom-in images of top and front views; right: zoom-out images). Scale bars: 100 nm.

Discussion

Like many concept schemes in the field of structural DNA nanotechnology, it is rationally sound to foresee that a systematic and comprehensive investigation of DNA nanostructures composed of various types of mesojunction building blocks for designer self-assembly, like canonical assemblies with regular junctions, was sorely needed. Based on the classic construction schemes that we adopted, we have successfully demonstrated the self-assembly of mesojunction-based lattices, including 1D periodic lattices, as well as 2D and 3D discrete and composite lattices. Discrete lattices also produce comparable assembly yield (8% - 82%).

Striking similarities can be observed between mesojunction-based lattices and regular junction-based lattices. For example, similar weaving patterns are presented in both mesojunction and regular junction lattices; structural deformation is presented in both architectures; and the toolbox of regular junction-based lattice self-assembly is useful in the formation optimization of mesojunction-based lattices. On the other hand, the routing patterns and strand topologies of mesojunction-based lattices are different to those of the regular junction-based counterparts. Differences have been previously reported in

stacking interaction at regular junction/mesojunction points and electrostatic repulsion among neighboring arms^{21, 22, 25}. The stacking interaction between mesojunction arms can induce a variable equilibrium among conformers by adjusting the arm length, as also suggested in the earlier studies.

It seems as if the mesojunction architecture existed in an alternate universe parallel to the one in which regular junction-based architecture was extremely well developed. The DNA nanostructures with such an unprecedented level of complexity and order demonstrated in the field are mostly based on regular junction. However, a structural design language with only one critical branching element is limited, and constraining structure inherently constrains the ensuing functional library that can be accessed. Specifically, regular junctions are geometrically driven by stacking interactions between opposing helices²⁵. Alteration of the junction sequence can be exploited by careful study in order to drive crossing angles with high precision, but inaccuracies can lead to torsion, bundling, or junction disruption in unanticipated ways²⁶. Presumably, the mesojunction design universe of DNA nanotechnology would be less dependent on stacking. This design strategy yields less-rigid structures but may — as we see in the lattices here — allow greater mechanical and rotational degrees of freedom. For example, the 4-arm designs will compensate the accumulation of major groove and minor groove and tolerate deviations from B-form twist. Moreover, there are more species of mesojunction configurations than junction/antijunction configurations for a complex with a fixed number of arms (e.g., 5-arm or 6-arm complexes)^{1,21}. This is an indication that there exists an uncharted design territory for structural DNA nanotechnology that is far more expansive than we earlier imagined. DNA nanotechnology was made possible by exploiting the immobile branched junction^{27, 28}, and four decades of study have elucidated its pivotal role in topological self-assembly. We present here a complementary dimension to this fundamental component; and we envision its use as a platform to produce constructs with increased complexity, hierarchical control with greater composability, and ultimately topologically driven designer functionalities.

References

- (1) Seeman, N. C. Structural DNA Nanotechnology; Cambridge University Press, 2016.
- (2) Fu, T. J.; Seeman, N. C. DNA Double-Crossover Molecules. Biochemistry 1993, 32 (13), 3211.
- (3) Winfree, E.; Liu, F. R.; Wenzler, L. A.; Seeman, N. C. Design and self-assembly of two-dimensional DNA crystals. *Nature* **1998**, *394* (6693), 539-544.
- (4) Mao, C. D.; Sun, W. Q.; Seeman, N. C. Designed two-dimensional DNA Holliday junction arrays visualized by atomic force microscopy. *Journal of the American Chemical Society* **1999**, *121* (23), 5437-5443.
- (5) LaBean, T. H.; Yan, H.; Kopatsch, J.; Liu, F. R.; Winfree, E.; Reif, J. H.; Seeman, N. C. Construction, analysis, ligation, and self-assembly of DNA triple crossover complexes. *Journal of the American Chemical Society* **2000**, *122* (9), 1848-1860.
- (6) Yan, H.; Park, S. H.; Finkelstein, G.; Reif, J. H.; Labean, T. H. DNA-Templated Self-Assembly of Protein Arrays and Highly Conductive Nanowires. *Science* **2003**, *301* (5641), 1882.
- (7) Liu, D.; Wang, M. S.; Deng, Z. X.; Walulu, R.; Mao, C. D. Tensegrity: Construction of rigid DNA triangles with flexible four-arm DNA junctions. *Journal of the American Chemical Society* **2004**, *126* (8), 2324-2325.
- (8) He, Y.; Ye, T.; Su, M.; Zhang, C.; Ribbe, A. E.; Jiang, W.; Mao, C. D. Hierarchical self-assembly of DNA into symmetric supramolecular polyhedra. *Nature* **2008**, *452* (7184), 198-201.
- (9) Yin, P.; Hariadi, R. F.; Sahu, S.; Choi, H. M. T.; Park, S. H.; LaBean, T. H.; Reif, J. H. Programming DNA tube circumferences. *Science* **2008**, *321* (5890), 824-826.
- (10) Zheng, J.; Birktoft, J. J.; Chen, Y.; Wang, T.; Sha, R.; Constantinou, P. E.; Ginell, S. L.; Mao, C.; Seeman, N. C. From molecular to macroscopic via the rational design of a self-assembled 3D DNA crystal. *Nature* **2009**, *461* (7260), 74.
- (11) Wei, B.; Dai, M.; Yin, P. Complex Shapes Self-Assembled from Single-Stranded DNA Tiles. *Nature* **2012**, *485* (7400), 623.
- (12) Ke, Y. G.; Ong, L. L.; Shih, W. M.; Yin, P. Three-Dimensional Structures Self-Assembled from DNA Bricks. *Science* **2012**, *338* (6111), 1177.

- (13) Wang, W.; Chen, S.; An, B.; Huang, K.; Bai, T.; Xu, M.; Bellot, G.; Ke, Y.; Xiang, Y.; Wei, B. Complex wireframe DNA nanostructures from simple building blocks. *Nature Communications* **2019**, *10* (1), 1067.
- (14) Rothemund, P. W. K. Folding DNA to create nanoscale shapes and patterns. *Nature* **2006**, *440* (7082), 297-302.
- (15) Dietz, H.; Douglas, S. M.; Shih, W. M. Folding DNA into Twisted and Curved Nanoscale Shapes. *Science* **2009**, *325* (5941), 725.
- (16) Douglas, S. M.; Dietz, H.; Liedl, T.; Hoegberg, B.; Graf, F.; Shih, W. M. Self-assembly of DNA into nanoscale three-dimensional shapes. *Nature* **2009**, *459* (7245), 414-418.
- (17) Han, D.; Pal, S.; Yang, Y.; Jiang, S.; Nangreave, J.; Liu, Y.; Yan, H. DNA Gridiron Nanostructures Based on Four-Arm Junctions. *Science* **2013**, *339* (6126), 1412.
- (18) Benson, E.; Mohammed, A.; Gardell, J.; Masich, S.; Czeizler, E.; Orponen, P.; Hogberg, B. DNA rendering of polyhedral meshes at the nanoscale. *Nature* **2015**, *523* (7561), 441-444.
- (19) Zhang, F.; Jiang, S.; Wu, S.; Li, Y.; Mao, C.; Liu, Y.; Yan, H. Complex Wireframe DNA Origami Nanostructures with Multi-Arm Junction Vertices. *Nat. Nanotechnol.* **2015**, *10* (9), 779.
- (20) Veneziano, R.; Ratanalert, S.; Zhang, K.; Zhang, F.; Yan, H.; Chiu, W.; Bathe, M. Designer nanoscale DNA assemblies programmed from the top down. *Science* **2016**, *352* (6293), 1534.
- (21) Du, S. M.; Zhang, S.; Seeman, N. C. DNA junctions, antijunctions, and mesojunctions. *Biochemistry* **1992**, *31* (45), 10955-10963.
- (22) Wang, H.; Seeman, N. C. Structural Domains of DNA Mesojunctions. *Biochemistry* **1995**, *34* (3), 920-929.
- (23) Seeman, N. C. Biochemistry and structural DNA nanotechnology: an evolving symbiotic relationship. *Biochemistry* **2003**, *42*.
- (24) Huang, K.; Yang, D.; Tan, Z.; Chen, S.; Xiang, Y.; Mi, Y.; Mao, C.; Wei, B. Self-Assembly of Wireframe DNA Nanostructures from Junction Motifs. *Angewandte Chemie International Edition* **2019**, *58* (35), 12123-12127.
- (25) Wang, W.; Chen, C.; Vecchioni, S.; Zhang, T.; Wu, C.; Ohayon, Y. P.; Sha, R.; Seeman, N. C.; Wei, B. Reconfigurable Two-Dimensional DNA Lattices: Static and Dynamic Angle Control. *Angewandte Chemie International Edition* **2021**, *60* (49), 25781-25786.
- (26) Simmons, C. R.; MacCulloch, T.; Krepl, M.; Matthies, M.; Buchberger, A.; Crawford, I.; Šponer, J.; Šulc, P.; Stephanopoulos, N.; Yan, H. The influence of Holliday junction sequence and dynamics on DNA crystal self-assembly. *Nature Communications* **2022**, *13* (1), 3112.
- (27) Seeman, N. C. Nucleic acid junctions and lattices. J Theor Biol 1982, 99 (2), 237-247.
- (28) Seeman, N. C.; Kallenbach, N. R. Design of immobile nucleic-acid junctions. *Biophysical Journal* **1983**, *44* (2), 201-209.